PNAS Nexus, 2022, 1, 1–12
https://doi.org/10.1093/pnasnexus/pgac048
Advance access publication date: 29 April 2022
Research Report

Geochemical ice-core constraints on the timing and climatic impact of Aniakchak II (1628 BCE) and Thera (Minoan) volcanic eruptions

Charlotte Pearson [a,b,c,*], Michael Sigl [d,e,*], Andrea Burke [f], Siwan Davies [g], Andrei Kurbatov [h,i], Mirko Severi [j], Jihong Cole-Dai [k], Helen Innes [f], Paul G. Albert [g] and Meredith Helmick [h,i]

[a]Laboratory of Tree-Ring Research, University of Arizona, 1215 E. Lowell Street, Tucson, AZ 85721, USA
[b]Geosciences, University of Arizona, 1040 E. 4th Street, Tucson, AZ 85721, USA
[c]Anthropology, University of Arizona, 1009 E. South Campus, Tucson, AZ 85721, USA
[d]Oeschger Centre for Climate Change Research, University of Bern, Hochschulstrasse 4, 3012, Bern, Switzerland
[e]Climate and Environmental Physics, University of Bern, Sidlerstrasse 5, CH-3012, Bern, Switzerland
[f]School of Earth and Environmental Sciences, University of St Andrews, Queen's Terrace, KY16 9TS, Scotland, UK
[g]Department of Geography, Faculty of Science and Engineering, Swansea University, Singleton Park, SA2 8PP, Cymru, UK
[h]Climate Change Institute, University of Maine, Orono, ME 04469-5790, USA
[i]School of Earth and Climate Sciences, University of Maine, 81 Main St., Orono, ME 04469-5790, USA
[j]Dipartimento di Chimica Ugo Schiff, University of Florence, Via della Lastruccia, 3, 50019 Sesto Fiorentino, Florence, Italy
[k]Department of Chemistry and Biochemistry, South Dakota State University, 1451 Stadium Rd, Brookings, SD 57007, USA
*To whom correspondence should be addressed: Email: c.pearson@ltrr.arizona.edu
Edited By: Efi Foufoula-Georgiou.

Abstract

Decades of research have focused on establishing the exact year and climatic impact of the Minoan eruption of Thera, Greece (c.1680 to 1500 BCE). Ice cores offer key evidence to resolve this controversy, but attempts have been hampered by a lack of multivolcanic event synchronization between records. In this study, Antarctic and Greenland ice-core records are synchronized using a double bipolar sulfate marker, and calendar dates are assigned to each eruption revealed within the 'Thera period'. From this global-scale sequence of volcanic sulfate loading, we derive indications toward each eruption's latitude and potential to disrupt the climate system. Ultrafine sampling for sulfur isotopes and tephra conclusively demonstrate a colossal eruption of Alaska's Aniakchak II as the source of stratospheric sulfate in the now precisely dated 1628 BCE ice layer. These findings end decades of speculation that Thera was responsible for the 1628 BCE event, and place Aniakchak II (52 ± 17 Tg S) and an unknown volcano at 1654 BCE (50 ± 13 Tg S) as two of the largest Northern Hemisphere sulfur injections in the last 4,000 years. This opens possibilities to explore widespread climatic impacts for contemporary societies and, in pinpointing Aniakchak II, confirms that stratospheric sulfate can be globally distributed from eruptions outside the tropics. Dating options for Thera are reduced to a series of precisely dated, constrained stratospheric sulfur injection events at 1611 BCE, 1561/1558/1555BCE, and c.1538 BCE, which are all below 14 ± 5 Tg S, indicating a climatic forcing potential for Thera well below that of Tambora (1815 CE).

Keywords: ice cores, tephra, sulfate, volcanic forcing, tree-rings

Significance Statement:

The date and climatic impact of the Minoan eruption of Thera have long been a focus of controversy. Key evidence lies in layers of volcanic sulfate and ash deposited in Greenland and Antarctic ice-sheets. Analysis of ice-core sulfuric acid can reveal the extent of climate system forcing from past volcanic aerosols, which redistribute solar energy and decrease warming at Earth's surface. Ash geochemical data from the same event layer can connect to a specific volcano. We synchronize continuous ice-core records, 1680 to 1500 BCE, defining and dating eruptions across the period to confirm high sulfur yield/climatic forcing for Aniakchak II at 1628 BCE, and confining Thera to one of a range of precisely dated lower sulfur/climate forcing events.

Introduction

For the last 2,500 years, correlations between the record of volcanic sulfate in Northern Hemisphere ice cores, and growth anomalies in tree-rings indicating sudden, short-term perturbations of the climate system, are well-established (1), allowing for detailed investigations of volcanic impact on human societies (2). Exact dating of such events is of the upmost importance because multiple timelines can often be secured and

Competing Interest: The authors declare no competing interest.
Received: September 16, 2021. **Accepted:** April 23, 2022

linked using volcanic marker horizons, enhancing understanding of cause and effect. Further back in time, this relationship is less accurately and precisely resolved, and controversies remain over when, where, and what impact, certain eruptions had on ancient societies and ecosystems.

The Minoan eruption of Thera, (Santorini) in the Mediterranean Sea, and the period c.1680 to 1500 BCE, have long been a focus of such investigation (3–7). This eruption, one of the more explosive of the Holocene (VEI 7 (8)), sealed the spectacular Minoan settlement of Akrotiri (on Thera) under meters of volcanic debris (9), and deposited tephra and other volcanic products across the wider region (10). The resulting marker horizon provides an important synchronization point for chronologies of the ancient Aegean, Anatolia, Levant, and Egypt, but dating it precisely has proved difficult. Archaeological connections between these regions, founded on the historical chronology of Egypt, indicate that the eruption must have occurred after the start of the New Kingdom (11–14). This is conventionally c.1540 to 1500 BCE (at earliest c.1560 BCE (13) or 1550 BCE (11)) or after 1570 to 1544 cal BCE (95.4% probability) based on radiocarbon dating (15). However materials buried by the eruption on Thera have been argued to radiocarbon date closer to 1600 BCE (16–18). This discrepancy can be partially explained by the impact of a radiocarbon plateau between c.1610 and 1540 BCE (19) and differences in approach to calibration and interpretation of materials buried by the eruption (20, 21). A range of factors related to potential radiocarbon reservoir effects, including volcanic contamination with 'old carbon' have also been suggested for material which grew on the island (12). A recent study on samples from a Theran tsunami deposit indicates a radiocarbon based date that is sometime 'after 1611 BCE' (10), with a seed found in this deposit, in close proximity to the first human remains associated with the eruption, yielding calibrated probability distributions of 1612 to 1573 cal BCE (19.4%) and 1665 to 1501 cal BCE (76.1%) (10). This illustrates the problematic nature of radiocarbon calibration in the period, but also possibilities for overlap with the New Kingdom.

Ice-core evidence from both poles offers the potential to refine the dating for Thera with much more accuracy, but incongruous dating schemes for different ice cores and evidence for multiple eruptions c.1680 to 1520 BCE (22–24) have limited progress. For example, the caldera forming Aniakchak II eruption (Alaska) has been geochemically confirmed in association with differently dated sulfate events in several Greenland ice-cores (25–27) with possible dating solutions proposed (7). Radiocarbon evidence for this event has previously been hampered by large associated errors (28, 29), making it temporally indistinguishable from Thera, however, reservoir corrected dates from marine mollusks in a tightly constrained sediment core (30) support a date of 3572 ± 4 years BP (c.1623 ± 4 BCE).

Between 1680 and 1520 BCE, a number of calendar dated tree-ring growth anomalies have been identified (3–6, 19, 40–43). Of these, the strongest, best replicated signal occurs in 1628/7 BCE (3–5, 42, 44). This has long been associated with the eruption of Thera (3, 4), but recently presented as a more likely candidate for Aniakchak II (7). Other, less strongly confirmed indicators for a potential volcanic impact highlight the years 1654/3 BCE (5–7), 1560 BCE (19, 42, 43), 1554 BCE (40), 1550BCE (42), 1546 and 1544 BCE (19), and 1524 BCE (6, 41).

To address these chronological, climate forcing, and volcanic attribution issues, we bring together Greenland and Antarctic records, synchronizing continuous high-resolution sulfur (395 BCE to 2006 CE) (45) and sulfate (4059 BCE to 395 BCE) (35) data using layer counts, and securing this in time with dendroclimatological age constraints (7). We present a comprehensive sequence of volcanic sulfate deposition 1680 to 1520 BCE and use these combined, securely dated, highly resolved data to provide additional constraints on the magnitude of sulfur injection, atmospheric sulfur life cycle, and potential source locations of the identified events. We also selected two events for high-resolution sampling, across multiple ice-core records, in order to search for tephra, clarify the association of any tephra found relative to the sulfate and, through sulfur isotope analysis, provide a more accurate estimate of the fraction of sulfate that was transported via the stratosphere (46) to improve stratospheric sulfate loading estimates. These data, along with geochemical analysis of the tephra recovered, are used to reveal consequential insights into the dating, size, and climatic forcing potential of Aniakchak II and the Minoan eruption of Thera.

Results

Synchronizing Northern and Southern Hemisphere ice-cores

Sulfate (and conductivity) peaks in Greenland (GISP2 (31), GRIP (32), NGRIP (27), and EGRIP (33)) and Antarctica (WDC (35) and EDML (36)) were aligned to calendar dated tree-ring events in 1654/53 BCE and 1628/7 BCE (see Fig. 1, Table 1; Figures S1 to S3 and Tables S1 and S2, Supplementary Material; Materials and Methods). Despite offsets in the previous absolute ages for this double sulfate signal in different records, the number of identified annual-layer markers between them in GRIP (26) and GISP2 (26) are in agreement with the number (26) obtained for WDC, allowing for a buffer of ±1 year to account for the atmospheric lifecycle between eruption and deposition on the ice sheets. The Irish tree-ring climatic response date of 1628 BCE (4, 7) was used to anchor the global ice-core chronology at this point in time, with 1 year dating uncertainty between the oak growth response and that of North American bristlecone pines (1627 BCE) linked to the unknown season of the eruption and the main growth period of the different tree-ring records. During the Common Era, maximum cooling and tree response occurs in the year of, or 1 year after an eruption (1, 5), so here we assume the onset of impact is represented by the year 1628 BCE. This synchronization confirms previous assertions that the GICC05 record requires a dating adjustment (7, 49). It also aligns a number of previously published tree-ring marker years with periods of sulfate deposition (Fig. 1), strengthening a volcanic causal hypothesis in each case. The main peaks in sulfate, and/or conductivity within this dated framework were assigned V1 to V7 (old–young) to improve navigation across events that were previously associated with different chronological schemes (Table 1). Previous tephra geochemistry data (25, 27, 38, 39), was assigned to the correct sulfate events within this framework (Fig. 1) connecting Aniakchak II (27) with V2. V2 and V5 were selected for high-resolution tephra and sulfur isotope sampling to provide further insights.

Source latitudes and sulfur injection

Eruption signals V1 to V7 (Fig. 1; Figures S1 to S3 and Tables S1 and S2, Supplementary Material) were assigned source latitudes on the basis of signal strength in respective Northern and Southern Hemisphere records, duration, and spatial distribution (Table 1, Fig. 2). Contemporaneously recorded volcanic acid signals in both poles of comparable magnitude and duration (2 to 3 years), are typically indicative of volcanic eruption sources in the lower latitudes. Short-duration spikes of acid recorded only

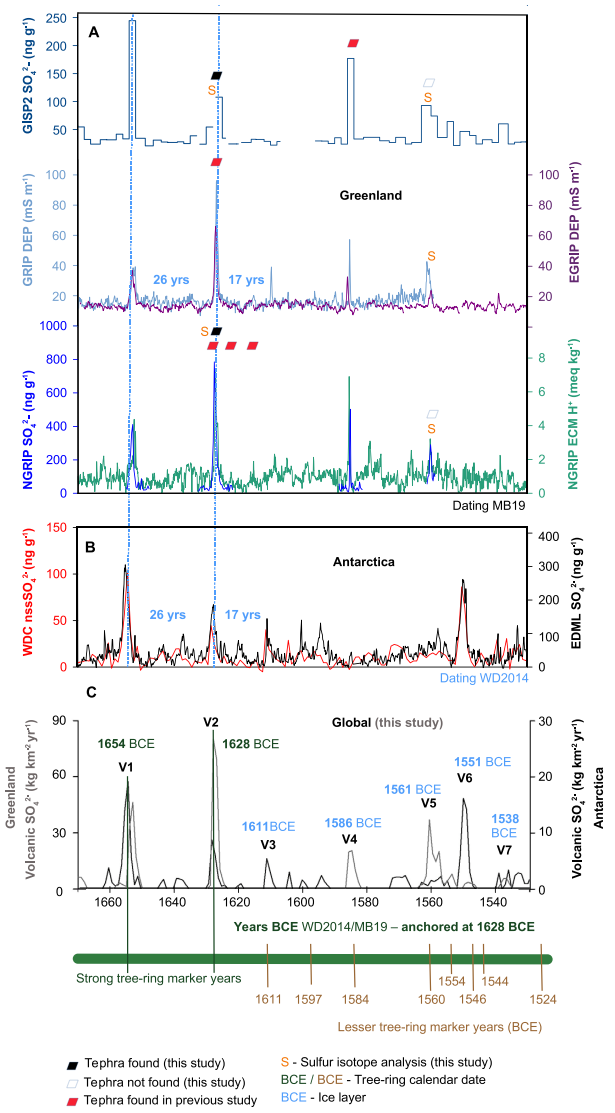

Fig. 1. Ice-core synchronization (blue vertical lines) using layer counts between bipolar volcanic aerosol records from Greenland (A) and Antarctica (B) and calendar dated tree-ring counts between climatic markers (C), anchored at 1628 BCE (7). V1 to V7 were assigned to aid navigation across key events discussed in the text. (A) Northern Hemisphere; GISP 2—Greenland Ice-Sheet Project (31); GRIP—Greenland Ice-Core Project (32), EGRIP (East) (33), and NGRIP (North) (27): (B) Southern Hemisphere; WDC—West Antarctic Ice-Sheet Divide ice core (34, 35), EDML—EPICA Dronning Maud Land ice core (36): EDML was volcanically synchronized to the annual-layer counted chronology (WD2014) of WDC. A shift of +1 year (i.e. toward younger ages) is necessary at 1628 BCE to anchor WD2014 with the tree-ring chronology (7), whereas +14 years (MB19) were used to align the Greenland GICC05 chronology with the tree-ring chronology. Previous tephra associations (25, 27, 37–39) and tephra recovered in this study are shown relative to the new synchronization. GISP2, NGRIP, and GRIP were resampled for tephra and sulfate across V5, GISP2, and NGRIP across V2.

in one hemisphere are typically indicative of eruptions from the high-latitudes of each respective hemisphere (45). Table 2 (Table S4, Supplementary Material), shows reconstructed volcanic sulfur injection (Tg S) based on cumulative volcanic sulfate deposition in Greenland and Antarctica, and on asymmetry ratios based on the mean distribution of historic volcanic eruptions (VEI ≥ 4) with tephra source confirmation (see Material and Methods). In depth sulfate analysis revealed five additional small events within the time period (Table 2, Fig. 2). Figure 2 shows sulfur injection calculations (Tg S) and asymmetry ratios for all events 1680 to 1500 BCE, relative to various dating possibilities for Thera (36.4°N). V2, V5, and V7 likely derive from a latitude of 30° to 60°N. V4 is consistent with a high latitude Northern Hemisphere eruption (60° to 90°N), V6 with a Southern Hemisphere extratropical event (30° to 90°S). V1 and V3 currently appear most consistent with a tropical (30°S to 30°N) source, however asymmetry indicates V1 may also be a Northern Hemisphere extra tropical eruption, and V3 could have derived from contemporaneous Northern and Southern Hemisphere events. Further analysis is required in both cases.

Sulfur injection calculations (see Materials and Methods) for sulfate deposition events across the study period were compared with historic volcanic eruptions of known origin (Fig. 3, Table 2). This showed that total sulfur injections for V1 (50 ±13 Tg S) and V2 (52 ±17 Tg S) exceed ice-core estimates for Tambora 1815 CE (34 ±7 Tg S), and likely exceed or at least equal Okmok II in 43 BCE (48 ±15 Tg S). Both of these latter eruptions resulted in significant climatic impacts for contemporary human populations (2, 61) so the implications for V1 and V2 are clear. The third largest sulfate event within the study period is V5 at 1561 BCE. At 22 ±7 Tg S this event is half way between Tambora and Krakatau (1883 CE) in scale. If V3 is indeed one low-latitude eruption (which requires further analysis) at 8 ±2 Tg S it would be similar in scale to Krakatau. V7 (6 ±2 Tg S) and other smaller sulfate markers not utilized in the initial synchronization (e.g. c.1558 BCE) are also of similar or lower sulfur injection to Krakatau.

Tephra evidence

Ice-core samples from GISP2 and NGRIP encompassing V2 yielded volcanic glass shards. Geochemical analyses of the NGRIP 641.12 to 641.16 m (n = 7) and GISP2 774.53.774.78 m (n = 16) cryptotephra deposits revealed a dominant and relatively homogeneous rhyolitic glass population which straddles the calc-alkaline to high-K calc-alkaline series boundary (Fig. 4; Figure S5, Supplementary Material). The NGRIP 641.12 to 641.16 m glass compositions are entirely consistent with the composition and source interpretation previously reported for cryptotephra QUB1198 which spanned 640.95 to 641.15 m in NGRIP (27) (Figure S5, Supplementary Material). Major element analysis (Fig. 4; Figure S5, Supplementary Material) supports a correlation between both NGRIP 641.12 to 641.16 m and GISP2 774.53.774.78 m and the Aniakchak II caldera-forming eruption, whilst a chemical link to the products of the Minoan (Thera) eruption can be easily excluded. This is most strongly illustrated by the TiO_2 content of the glass shards (Figure S5C and D, Supplementary Material), where the rhyolitic tephra deposits (Aniakchak II) preserved in Greenland display higher TiO_2 content compared to the glass compositions of the Minoan eruption products. Sampling was conducted at a higher temporal resolution than previous studies (27) and confirmed a clear association of the cryptotephra with the initial rise of the V2 stratospheric sulfate deposition (Fig. 5). This distinct stratigraphic position in the ice-core mirrors that of comparable mid-latitude eruptions (Okmok II, Taupo-Oruanui) identified recently in polar ice cores at high depth-resolution (2, 66). No tephra was found from samples encompassing the V5 event in Greenland. We also report no tephra resulting from a search of the well-dated, mid-latitude Tsambagarav ice core (67) (Mongolian Altai, 4130 m asl, 48.7°N, 90.9°E), which, c.5,000 km downwind of Thera, might have greater potential to capture volcanic ash particles transported by westerlies than the Greenland ice.

Table 1. Dating for events V1 to V7 relative to depth and dating scales applied to the Greenland and Antarctic records (Fig. 1). Ages in brackets are based on linear interpolation between volcanic age markers on the WDC timescale, or based on extrapolation of the 14-year time transfer suggested by (7). *There was no archived ice left across the V2 event in GRIP at this depth. Blanks indicate 'not present'. Exact tephra depths in GISP2, GRIP, and NGRIP are provided in Table S3 (Supplementary Material). Source attributions are banded as follows: NH_{high} = 60° to 90°N, NH_{ext} = 30° to 60°N, tropical = 30°S to 30°N, and SH_{ext} = 30° to 90°S

	V1	V2	V3	V4	V5	V6	V7	Refs.
GISP2 depth (m)	778.82	774.52	–	766.88	762.94	–	759.07	(31)
GRIP depth (m)	740.56	736.47*	733.55	729.51	725.47	–	–	(32)
NGRIP1 depth (m)	644.86	641.02	638.17	634.7	630.99	–	627.67	(27)
WDC depth (m)	850.73	845.08	841.38	–	–	828.56	–	(34,35)
EDML depth (m)	272.3	270.72	269.61	–	–	265.78	–	(36)
Age $(BCE)_{Meese}$	1695	1670	–	1624	1600	–	1577	(48)
Age $(BCE)_{GICC05}$	1667	1641	1624	1599	1574	–	1552	(47,60)
Age $(BCE)_{WD2014}$	1656	1629	1612	(1584)	(1562)	1551	(1538)	(34)
Age $(BCE)_{IntCal13}$	1647	1622	1605	1580	1555	NaN	1532	(49)
Age $(BCE)_{MB19}$	1653	1627	(1610)	(1586)	(1561)	–	(1538)	(7)
Age (BCE)	1654	1628	1611	1586	1561	1551	1538	This study
Source attribution	Tropical/ NH_{ext}	Aniakchak NH_{ext}	Tropical/ NH_{ext}/SH_{ext}	NH_{high}	NH_{ext}	SH_{ext}	NH_{ext}	

Sulfur isotopes

Mass independent fractionation (MIF) of sulfur isotopes occur when erupted sulfur is exposed to ultraviolet radiation, i.e. when an eruption plume reaches altitudes in the stratosphere at or above the ozone layer (56). As such, the presence of a MIF signal in an ice-core sulfate layer indicates that at least some of the sulfate came from the stratosphere and can, therefore, be used to confirm stratospheric events or to distinguish a bipolar event from two separate hemispheric events that occur within age uncertainty of each other (46). Sulfur isotope analysis of V2 (Aniakchak II) shows a signal that begins (up to 100 ng/g) with an isotopic pattern consistent with a high latitude source, showing sulfate that came from below the ozone layer (Fig. 5; Figures S6 and S8, Supplementary Material). $\delta^{34}S$ and $\Delta^{33}S$ trends at the beginning of the sulfate peak are similar to those recorded from the Katmai/Novarupta 1912 eruption (46), with an initial decrease in $\delta^{34}S$ and a $\Delta^{33}S$ value within error of zero, consistent with the Alaskan origin of Aniakchak II. This pattern is reproduced in two high time-resolution records of $\Delta^{33}S$ from sulfate deposited at two different ice-core sites in Greenland (NGRIP and GISP2) adding confidence to these results. In contrast to the Katmai eruption, a large proportion of the rest of the acidity peak is stratospheric, and as such, the measured $\Delta^{33}S$ values for this event in both cores are greater than 1‰, more similar to values seen in tropical eruptions that deposit purely stratospheric sulfate on the ice sheets (46). This value is larger than previous reported results for extratropical events (typically around 0.4‰, (46)), indicating that the event expelled an unusually large amount of sulfate high into the stratosphere and there was relatively little tropospheric transport to Greenland. Isotope mass balance (46) in the NGRIP core also shows a pronounced peak in sulfate from below the ozone layer after the peak in stratospheric sulfate. The signature of a single extratropical eruption would typically result in a peak in tropospheric derived sulfate before the peak in stratospheric sulfate (which tends to occur c. 6 months after the eruption (68)) reflecting the differences in atmospheric residence time (tropospheric being shorter). The tropospheric (or more precisely, "below ozone") peak following the stratospheric peak in NGRIP supports the idea of a second lesser explosion, backed up by the occurrence of more than one Aniakchak tephra fall in the ice (27), or a small eruption from a similar latitude volcanic source. In GISP2, the distinction between the stratospheric and "below ozone" peak is less defined, possibly because GISP2 was sampled at 5 cm resolution and NGRIP at 4 cm resolution, but similarly the main "below ozone" component does not arrive prior to the stratospheric component. No sulfur isotope analyses have yet been performed for the corresponding

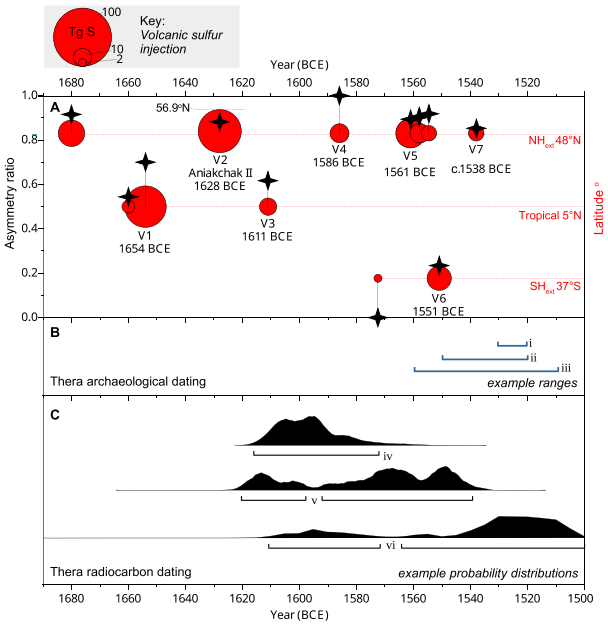

Fig. 2. (A) Reconstructed volcanic sulfur injection (Tg S, Table 1), based on cumulative volcanic sulfate deposition in Greenland and Antarctica, plotted according to default eruption latitudes derived from the mean distribution of known source historic eruptions VEI ≥ 4, where asymmetry ratios > 0.75 = 48°N; < 0.25 = 37°S; and all others = 5°N. Black stars show asymmetry where 0.5 is equal distribution in both hemispheres. All eruptions ≥ 2 Tg S are shown, including a possible candidate for Mt. St Helens Yn at 1680 BCE. (B) Archaeologically derived dates for Thera; (i) several decades after the start of the New Kingdom in Egypt (11, 12); (ii and iii) 'after' the start of the New Kingdom (11) and (13). (C) IntCal20 calibrated radiocarbon dates from Theran contexts; (iv) Thera olive, 25% uncertainty, (v) Thera olive, ordered sequence (16, 19); (vi) Çeşme-Bağlararası tsunami seed (10). Dating possibilities presented illustrate the problems of dating Thera, compounded by a radiocarbon plateau, subjective decisions in modeling and different interpretations of the evidence (19–21).

Table 2. Eruption dates and cumulative sulfate SO_4^{2-} deposition at ice-core sites in Greenland and Antarctica for V1 to V7, with five additional events revealed through new analysis and three more recent analogues with known source and date. Dating is given according to known calendar dates or dates applied in this study. 'GRL Mean' includes mean sulfate deposition from Dye 3 and GRIP (23) for V2 (Aniakchak II) V3, Okmok II, and Tambora. [a] indicates association with a bristlecone pine frost-ring within ±1 year of ring-width minima in 43 BCE, 1627 BCE, and 1653 BCE (5). Blanks indicate 'no data'. [b] sulfur injections are 3 (±1) and 2 (±1) Tg for the alternative attribution scenario of two distinct eruptions. Due to the low temporal resolution in GISP2 and discontinuous sampling in NGRIP, the volcanic sulfate deposition for V3, evident in electrical records from NGRIP and EGRIP (33) was estimated based on published discontinuous data from the GRIP and Dye-3 ice core (23).

Eruption date	$f_{GRL\ Mean}$ SO_4^{2-}	f_{GISP2} SO_4^{2-}	f_{NGRIP} SO_4^{2-} [kg km^{-2}]	f_{ANT} SO_4^{2-}	f_{WDC} SO_4^{2-}	f_{EDML} SO_4^{2-}	Asymmetry $\frac{f_{GRL}}{(f_{GRL}+f_{ANT})}$	Source	SO_4^{2-} burden	Sulfur Injection [Tg S]
1883 CE	22	29	15	16	21	11	0.59	Krakatau	Bipolar	13 ± 3
1815 CE	36	54	40	65	87	44	0.35	Tambora	Bipolar	34 ± 7
43 BCE	117	123	122	20	24	15	0.86	Okmok[a]	Bipolar	48 ± 15
1539 BCE	16	16	–	3	6	0	0.85	V7	Bipolar	6 ± 2
1550 BCE	12	12	–	40	44	36	0.23	V6	Bipolar	17 ± 3
1555 BCE	17	17	–	17	0	37	0.92		Bipolar	6 ± 2
1558 BCE	27	27	–	3	0	6	0.90		Bipolar	10 ± 3
1561 BCE	57	91	70	7	0	15	0.89	V5	Bipolar	22 ± 7
1573 BCE	0	0	0	10	19	0	0.00		SH	2 ± 1
1586 BCE	55	79	30	0	0	0	1.00	V4	NH	10 ± 4
1611 BCE	16	0	–	10	15	5	0.62	V3	Bipolar?	8 ± 2[b]
1628 BCE	137	185	147	19	16	22	0.88	Aniakchak[a]	Bipolar	52 ± 17
1654 BCE	105	120	91	45	52	38	0.70	V1[a]	Bipolar	50 ± 13
1658 BCE	8	8	–	7	6	8	0.54		Bipolar	5 ± 1
1678 BCE	55	55	–	5	6	4	0.92		Bipolar	20 ± 7

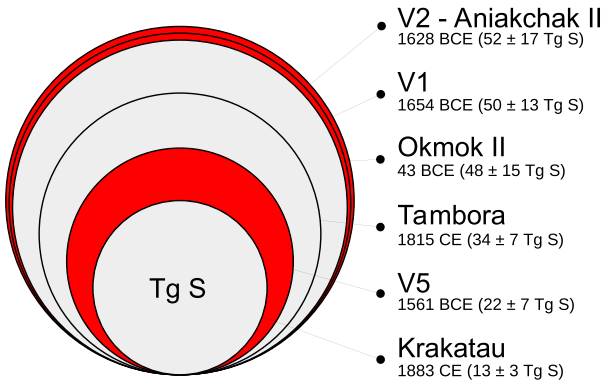

Fig. 3. Comparison of V1, V2, and V5 sulfur injections (Tg S) with previous known age eruptions of wide ranging impact.

sulfate peak in 1629 BCE in Antarctica, but the duration of volcanic sulfate deposition of more than 2 years is typical for stratospheric input from a non-local source.

Sulfur isotope data for V5 in both GISP2 and GRIP show a muted stratospheric MIF signal ($\Delta^{33}S$ around 0.3 to 0.4‰; Fig. 5; Figures S7 and S8, Supplementary Material). In GRIP, the signal is consistent with an extratropical eruption, as the $\delta^{34}S$ values decrease at the start of the peak but the $\Delta^{33}S$ values remain within error of 0‰, and this is followed by a small, but significant, nonzero $\Delta^{33}S$ value in the latter part of the peak. In GISP2 (Figure S7, Supplementary Material), on the other hand, there appears to be two sulfate peaks over this time interval: a larger one reaching 300 ppb sulfate followed by a smaller one reaching 150 ppb sulfate. We sampled the large peak and only the start of the smaller peak in this record, thinking the larger peak correlated with the signal in GRIP. The large peak, however, had no stratospheric sulfate in it. This suggests that the smaller peak, which has a muted stratospheric MIF signal, in fact correlates with the signal in GRIP, and that two eruptions may have occurred. NGRIP results similarly indicate that ice-sampling may have missed the second (stratospheric) sulfate signal.

Discussion

Based on the current available evidence (Fig. 2) we assign; V1 (1654 BCE) to a high sulfate, unidentified NH low-to-mid latitude eruption, too old for Thera (10), possible, though a little young (69) for the Mt. St Helens Yn eruption (the highest intensity and largest magnitude Mt. St Helens eruption in postglacial times (70)) and no longer associated with the Aniakchak II tephra; V2 (1628 BCE) to Aniakchak II, confirmed in this study in clear association with the peak in stratospheric sulphate; V4 (1586 BCE) to an unidentified high latitude Northern Hemisphere event distinctive from Thera, Mt. St Helens, Vesuvius, or Icelandic source volcanoes based on tephra geochemistry (71); and V6 (1551 BCE) to an unidentified Southern Hemisphere event.

V3 (1611 BCE), V5 (1561 BCE), V7 (c. 1538 BCE), and additional events revealed at 1558 and 1555 BCE require further investigation. The Minoan eruption of Thera had an estimated column height of c.36 ±5 km (72), which at 36.4°N, should have breached the tropopause and deposited c. 2 to 3 years sulfate signals in both poles, with larger sulfate mass deposition in Greenland than in Antarctica. The eruption occurred in the summer (73), which according to model simulations (74) would increase the chances of Antarctic deposition. Based on upper sulfur yield estimates for Thera (35.9 Tg S (72)), V5 (1561 BCE) initially stood out as the strongest candidate within this group, however, the range for such estimates is very wide (0.34 Tg S at lowest (72)), and the summarized dating complexities (Fig. 2) mean all remaining bipolar events require further examination.

V3 (1611 BCE) is consistent with a single, lower latitude event (30°S to 30°N), but the short duration of the sulfate deposition in Greenland and its large spatial variability (seen at some sites,

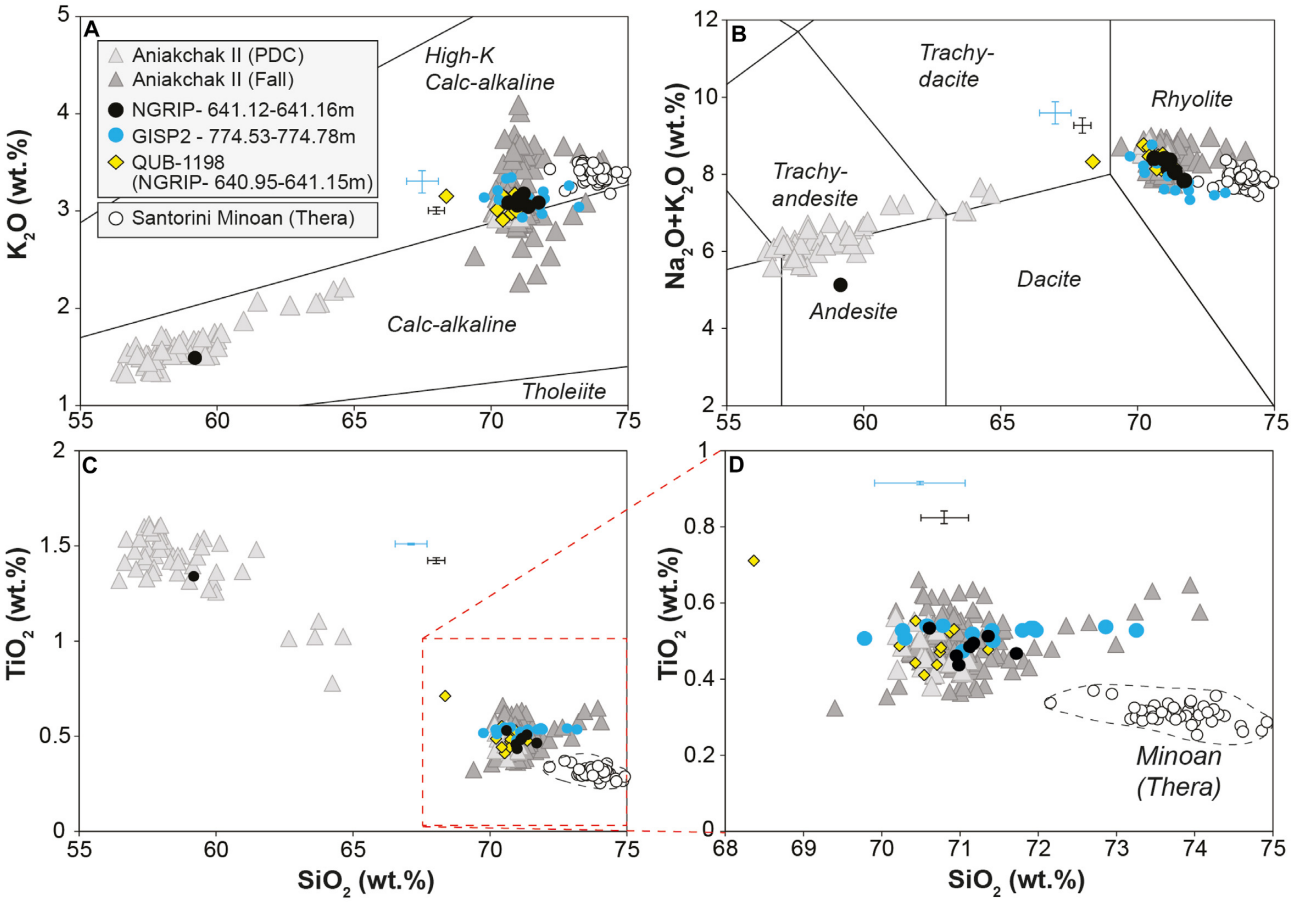

Fig. 4. Major and minor element analyses of volcanic glass shards identified in NGRIP 641.12 to 641.16 m and GISP2 774.53 to 774.78 cryptotephras (V2), compared to previous analyses of the QUB-1198 tephra (27), and the proximal volcanic glasses of deposits erupted during the caldera-forming Aniakchak II (62) and Minoan (Thera) eruptions (63). Black error bars represent 2 SDs of replicate analyses of the ATHOG MPI-DING (64) glass standard run alongside the NGRIP 641.12 to 642.16 m sample, whilst blue error bars represent 2 SDs of replicate analysis of the NMNH 72854 (65) glass standard run alongside GISP2 774.53 to 774.78 m. Full chemical datasets including secondary standards are provided in the Supplementary Material.

absent at others) is more characteristic for an extratropical eruption. In this case, the signal might be explained by contemporary Northern and Southern Hemisphere eruptions. The dated position for V3 aligns with certain long-held radiocarbon arguments based on materials buried by Thera (16–18), but not with archaeological evidence for a date after the start of the New Kingdom in Egypt (11, 13, 41). It also corresponds with the onset of a uranium series dated chemical marker in Sofular cave, Türkiye (75). The slightly higher latitude V7 sulfate (c.1538 BCE), is not so accurately dated as the other signals due to ice quality, but does offer a better fit with the archaeologically based dating for the New Kingdom / Thera (11, 41, 76), and may yet link to a range of less substantiated tree-ring responses reported in the 1540's BCE (19, 43). Further work is required on both of these events. We note that the Antarctic ice shows no major signal that would support a larger bi-polar event around 1524 BCE, when narrow growth in bristlecone pine (77) (Fig. 1) has also been proposed for Thera (11, 41), but current data gaps in GRIP, GISP2, and NGRIP make this harder to explore in Greenland.

The V5 sulphate beginning at 1561 BCE appears to be from a latitude consistent with Thera and corresponds with a previously reported chemical change in East Mediterranean tree-rings between c.1562 and 1558 BCE (43), an isotopic signal consistent with volcanic haze in Finland pines (42), and increased sulfur deposition in Sofular cave (75). It is not marked by a frost ring in North American Bristlecone pine (for which the strongest volcanic forcing connection is established (1)), but rather by reduced growth at 1560 BCE in that species (19), consistent with lower sulfur injection estimates for this event. The 22 ±9 Tg S calculated, of which 64 ±9% or 14 ±5 Tg S reached the stratosphere in the later part of the signal, places this sulfate deposition mid-way in size between Krakatau (13 ±3 Tg S) and Tambora (34 ±7 Tg S; Fig 3). This is consistent with proportions of petrographically estimated H_2SO_4 (78), which place the Minoan eruption of Thera between these two events. The longer duration signal and strong asymmetry of sulfate deposition toward the Northern Hemisphere is consistent with what might be predicted for Thera, but sulfur isotopes show that the early part of the signal is mostly tropospheric with the stratospheric sulfate emerging toward the end of the sampled section. This may be consistent with combined archaeological and geological evidence for significant precursory eruptive activity preceding the Minoan eruption (9)), however, it could also, perhaps more likely, relate to two different source volcanoes, with the stratospheric signal as a candidate for Thera and the tropospheric signal from a source closer to Greenland. The combined sulfate records also revealed two additional bipolar, lower sulfur events at 1558 BCE (10 ±3 Tg S) and 1555 BCE (6 ±2 Tg S; Fig. 2, Table 2) which provide important avenues for further investigation. 1555 BCE aligns with a tree-ring event (1554 BCE) in trees from Siberia (40), which may indicate a different source latitude to the 1561 BCE and 1558 BCE sulfates.

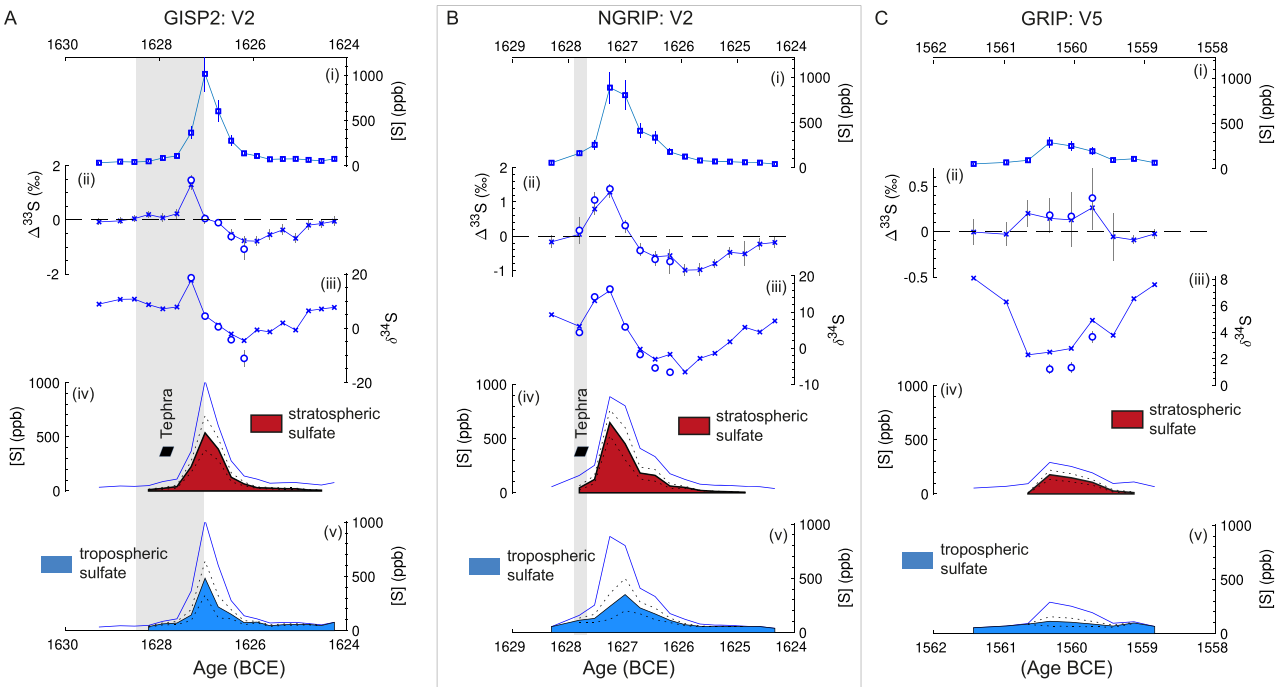

Fig. 5. Sulfur concentration, isotopes, and proportion of stratospheric and tropospheric sulfur from V2 in the GISP2 (A) and NGRIP (B) and V5 in GRIP (C). Each panel illustrates: (i) sulfur concentration (ppb), (ii) measured $\Delta^{33}S$ in all samples (x's) as well as $\Delta^{33}S$ of volcanic sulfate (o's), corrected for background sulfate with isotope mass balance for samples with greater than 65% sulfate derived from volcanic sources (see Methods), (iii) same as (ii) but for $\delta^{34}S$, (iv) sulfate concentration with the calculated proportion of sulfate deposited via the stratosphere (red), and (v) same as (iv) but blue denotes sulfate that remained below the ozone (mix of background and volcanic sulfate from low atmospheric altitudes). Dotted lines show uncertainties. Tephra shards were found between NGRIP 641.16 and 641.08 m in this study (1627.9 to 1627.9 BCE, see gray vertical bands) partially overlaping in depth with QUB-1198. QUB-1201 (not replicated here), was found between 641.50 and 641.70 m (1631.7 to 1630.5 equivalent).

While evidence presented in this study appears to best converge on the 1561 BCE sulfate for Thera, counter arguments in terms of archaeological and radiocarbon dating schemes make further high-resolution sulfate analysis and tephra sampling across V3 to V7, and 1558/5 BCE in both hemispheres (and c.1524 BCE in Greenland) essential to provide clinching evidence to confirm the true date.

Geochemical analysis of tephra recovered from V2 (1628 BCE; Fig. 4) at the transition between the primary "below ozone" sulfate and the main peak in stratospheric sulfate (Fig. 5; Figures S6 and S8, Supplementary Material) shows clear agreement with the chemistry of QUB-1198/Aniakchak II, and may relate to the emplacement of pyroclastic density currents associated with the caldera-forming eruption. This strongly confirms the association of Aniakchak II with the single large stratospheric sulfate signal, indicating an unusually large and explosive event with primary stratospheric sulfate deposition, followed by a secondary, lesser eruption. This is consistent with other evidence for Aniakchak II as one of the largest explosive events of the Holocene (79), a multistage caldera forming eruption (80, 81) which deposited visible tephra 1,100 to 1,300 km from the source and cryptotephra over 4,500 km (79), producing a minimum bulk eruption volume of over 50 km^3.

The singular association of the V2 acidity with Aniakchak II challenges the previous practice of attributing bipolar signals to lower latitude eruptions and indicates that major caldera forming eruptions in the mid-latitudes may also be imprinted in Antarctic ice. This adds to an increasing body of evidence from precisely dated state-of-the art ice cores and aerosol modeling, which suggests that sulfate is globally distributed in the stratosphere following powerful eruptions located outside the tropics (2, 45, 74, 82). Furthermore, because the section containing the peak of the sulfate was previously missing in the discrete sulfate measurements from GISP2, and the bipolar nature of this event was not previously recognized, the radiative forcing from this eruption has been strongly underestimated (22, 83). Our estimate of 52 ±17 Tg S (or 104 Tg SO_2) is consistent with petrological estimates of a high sulfate event (24, 84) and corresponds with evidence of severe environmental acidification following Aniakchak II (28). Sulfur isotope analysis suggests that 61 ±6% of the sulfate deposited on Greenland derived from stratospheric transport. We, therefore, estimate that Aniakchak II produced a constrained stratospheric sulfur injection of 32 ±11 Tg S, ranking among the largest events of the Late Holocene (see Table 2; Table S4, Supplementary Material). The high fraction of stratospheric sulfate explains the strong and widespread tree-growth anomalies (4, 5, 7, 40, 42, 44, 77) consistent with the observed and simulated effects of major high latitude stratospheric eruptions on climate (2, 82).

Aniakchak II emerges as the major climatic forcing event of the period, closely preceded by V1, 1654 BCE. Both these eruptions, although within stated errors, appear to exceed the forcing capacity of Okmok II, an event which produced unusually wet and cold conditions in the Mediterranean region (2). While several studies have noted no significant climatic shifts in Mediterranean sequences immediately following Thera tephra (85) or pumice (86) (supporting our findings that Thera was an event of lower climatic forcing potential) there is a well-replicated climate shift in a variety of Mediterranean speleothem records around 3.6 ka BP (87). There is also a major environmental change around this time linked with the termination of the Arctic Norwegian Stone Age (88). These events should now be further investigated, because Aniakchak II at 1628 BCE may be the primary forcing, as well as

the source of the volcanic haze hypothetically described in the Babylonian observations of Venus (89).

New Greenland ice cores—offering for the first time excellent core quality though-out this time window (33), combined with the state-of-the art analysis techniques employed here have the best potential to further delineate the timing, sources, and climatic consequences of volcanic eruptions during this critical time period. Anchoring Greenland and Antarctic ice-core chronologies with dendrochronological precision for this period not only provides our new record of volcanic forcing, but also other key climate records extracted from these ice cores (e.g. solar forcing; greenhouse gas forcing; temperature, sea-ice, and others), which will increase our understanding of the drivers and amplitudes of late Holocene climate.

Materials and Methods

Ice-core synchronization

Over the past decades, several deep ice cores have been dated by counting intra-annual variations in impurity content and water isotopic composition. Various dating schemes for cross-correlation are shown in Table 1. The original layer-counted timescale of the Dye-3 ice-core in which the Thera eruption was proposed to have been identified at a depth (V2) then corresponding to 1645 BCE (37), was subsequently revised to 1641 BCE on GICC05 (47). This timescale was then transferred to other Greenland ice cores including GRIP and NGRIP. In the layer-counted GISP2 ice-core, the corresponding layer had an age of 1670 BCE (48). In the independently layer-counted WD2014 chronology from Antarctica (34), a sulfuric acid spike we attribute to derive from the same eruption is dated to 1629 BCE (35). This age is within errors synchronous with the acid spike observed in Greenland ice cores, when applying the age transfer based on $^{10}Be/^{14}C$ matching (49) as well as with the frost-ring formation and tree growth anomalies in the SW USA and in Ireland (7), respectively. The same holds true for the earlier volcanic signal (V1) and tree-ring signals dated to 1653 BCE. Layer counting confirmed a previous proposed age correction (7), placing all the volcanically synchronized ice-core records from Greenland (NGRIP, GISP2, GRIP, and EGRIP) on a floating chronology ('MB19') anchored by the climate/bristlecone pine frost-ring associations in 1653 and 1627 BCE. By doing this, we correct for dating bias accumulated over the past 3.6 ka while still respecting the layer boundaries and identified layering during this time window.

Sulfate injection estimates

Sulfate injection estimates were made on existing and new measurements of sulfate from four deep ice cores: NGRIP (27) and GISP2 (38); and WD2014 (35) and EDML (36) using established methods (50). We resampled and annualized the sulfate records by averaging all samples within a calendar year (NGRIP, WDC, and EDML), or by interpolation (GISP2). The nonvolcanic background sulfur concentration was initially approximated in the four ice cores with a 101-year (window) running median (RM) fit to the annual sulfate data. As a robust measure of the variability of the background in the presence of outliers, the median absolute deviation (MAD) from RM was obtained for each 101-year window. To detect volcanic events over the variable background, a threshold of RM+2 × MAD was adopted. A year was deemed to contain volcanic fallout if the annual sulfate concentration exceeded this threshold. Years with concentrations above the threshold were removed and the reduced running mean (RRM) was calculated for the remaining years in the 101-year window in the time series. The duration of the volcanic event is defined as the length of time in which the sulfate concentrations exceeded RM + MAD. Annual volcanic sulfate concentration is calculated as the difference between the total sulfur concentrations of that year and the RRM of the nonvolcanic sulfate of that year. The cumulative sulfate mass deposition rate (kg km$-^2$) by an eruption, often referred to as (cumulative) "volcanic sulfate flux", is the sum of annual volcanic sulfate fluxes in the years when volcanic deposition occurred, multiplied by annual ice accumulation rates at the sites. We derived mean Greenland (f_G) and Antarctica (f_A) cumulative sulfate mass deposition by averaging the estimates from GISP2 and NGRIP, and from WDC and EDML, respectively. The hemispheric partitioning of the atmospheric sulfate burden can contain information about plausible latitudes of past eruptions as an asymmetry factor $A_{sulfate}$ calculated using Eq. (1):

$$A_{sulfate} = \left[\frac{f_G}{(f_G + f_A)}\right]. \quad (1)$$

Stratospheric sulfate injections are estimated from the ice-sheets sulfate flux composites using a method described in detail by Toohey and Sigl (51). Briefly, Greenland (f_G) and Antarctica (f_A) are related to injected sulfur mass M_S following Eq. (2):

$$M_S = \frac{1}{3}[L_{NH} f_G + L_{SH} f_A], \quad (2)$$

where L_{NH} and L_{SH} are transfer functions accounting for the spatial distribution of sulfate deposition over each hemisphere. Based on analysis of the spread and deposition of radionuclides from nuclear bomb testing, sulfate from prior volcanic eruptions and atmospheric model simulations (52), the transfer functions L_{NH} and L_{SH} are estimated to be 1×10^9 km^2 for tropical eruptions and 0.57×10^9 km^2 for extratropical eruptions.

Assessing ice-core derived asymmetry factors (or ratios) for historic eruptions with known latitudes we attribute possible source latitudes for all unknown eruptions using an asymmetry factor of > 0.75 (< 0.25) to discriminate Northern (Southern) Hemisphere extratropic eruptions from low latitude eruptions, respectively. (See Figure S9, Supplementary Material, for details and additional references). Default latitudes were assigned within these three latitudinal bands based on the spatial distribution of Holocene eruptions (VEI ≥ 4).

Tephra

Tephra sampling and analysis were carried out according to tephra community best practice protocols (53), with full metadata supplied in supplementary information and supplementary data. Parallel longitudinal subsamples fully encompassing both acid signals for V2 and V5 4 cm^2 in cross-section were searched for tephra (Figure S4, Supplementary Material). Samples from GISP2 (at depths of 762.50 to 763.45 m and 774.10 to 774.95 m) in the NSF-ICF ice-core archive, were analyzed at the Ice Core Microparticle and Tephrochronology Laboratory, University of Maine, using established protocols (54). GISP2 samples were shipped frozen to the University of Maine, subsampled and precleaned with a surgical razor blade under clean room conditions and melted in Whirl-Pak® plastic bags. A total of nine sampling intervals (762.47 to 762.78 m, 762.81 to 762.88 m, 762.90 to 762.99 m, 763.02 to 763.19 m, 763.21 to 763.44 m, 774.01 to 774.295 m, 774.295 to 774.53 m, 774.53 to 774.78, and 774.80 to 774.99 m) were processed into epoxy mounts and coated with a 15-nm layer of carbon using an Emitech high vacuum evaporator. Volcanic glass particles

were identified in the 774.53 to 774.78 m interval using a Tescan Vega II XMU scanning electron microscope (SEM). Geochemical analyses were performed with a 40 mm^2 EDAX Apollo SSD 40 energy dispersive spectrometer (EDS). Concentrations of major and minor oxides were measured via secondary electron beam X-ray microanalysis with an accelerating voltage of 15 kV, focused beam (1 to 2 m) operated at a constant distance from the specimen with a count time of 100 live seconds. The net peak intensities were converted to oxide weight percent using the semiquantitative EDAX GenesisTM software. To improve analytical precision, mounts were polished and cleaned and eleven particles were analyzed using SEM–EDS and a Cameca SX-100 electron microprobe equipped with 5 wavelength dispersive spectrometers (WDS).

Samples from NGRIP (630.3 to 631.40 m and 640.2 to 641.3 m) and GRIP (724.9 to 726.0 m) depths and eight consecutive cross sections of 7 to 10 cm^2 from the Tsambagarav ice core 65.42 to 65.84 m (encompassing 1680 to 1460 BCE; see Figure S10 and Table S5, Supplementary Material) were processed at Swansea University using established methods (55). Samples were melted, centrifuged, and pipetted onto microscope slides, dried and embedded in epoxy resin. Major element compositions were determined using a wavelength-dispersive JEOL JXA-8200 electron microprobe equipped with five wavelength-dispersive spectrometers at the Research Laboratory for Archaeology and the History of Art, University of Oxford. A beam accelerating voltage of 15 kV was used with a 6 nA current and a defocused beam diameter of 5 μm. The instrument was calibrated with a suite of appropriate mineral standards; peak count times were 30 s for all elements except Mg (50), Mn (50 s), Na (12 s), Cl (50 s), and P (50 s). Reference glasses from the Max Plank institute (MPI-DING suite) bracketing the possible chemistries were also analyzed alongside the NGRIP tephra. Full details on accuracy and error, plus datasets and secondary standards for the tephra analysis are presented in supplementary information and in Data S6 to S13.

Sulfur isotopes

S-isotope analyses were made on discrete samples (cross-sections of 6 to 10 cm^2) cut from archived ice-core sections from GRIP, NGRIP, and GISP2 for event V5 and NGRIP and GISP2 for V2, including both prior background and full acid deposition. The sample resolution over these events is 4 to 5 cm corresponding to a nominal 3-month age resolution. Sulfate concentration was measured by ion chromatography on the discrete samples, and the sulfate was purified from the melted ice using anion exchange columns (46). Triple sulfur isotopes (^{32}S, ^{33}S, and ^{34}S) were measured on the samples using a Neptune Plus multicollector inductively-coupled mass spectrometer (MC-ICP-MS) at the St Andrews Isotope Geochemistry Lab (STAiG lab) and are reported as $\delta^{34}S$ and $\Delta^{33}S$ relative to Vienna-Canyon Diablo Troilite (V-CDT), where $\delta^{x}S = ({}^{x}S/{}^{32}S)_{sample}/({}^{x}S/{}^{32}S)_{V\text{-}CDT} - 1$. A sample is considered to have a MIF signature if it has a nonzero value of $\Delta^{33}S = \delta^{33}S - ((\delta^{34}S + 1)^{0.515} - 1)$, outside of 2σ uncertainty. This method (46) allows analysis of samples that are at least 100 times smaller than the typical light gas stable isotope measurement previously employed in ice-core studies (56, 57). Full procedural blanks and an in-house secondary standard (Switzer Falls (58)) were processed alongside samples. Blanks contained 0.19 ±0.09 nmol sulfate and had $\delta^{34}S = 4.9 \pm 2.7$ (2 SD, $n = 11$). Long-term reproducibility of the Switzer Falls standard at the STAiG lab is 0.12 for $\delta^{34}S$ and 0.11 for $\Delta^{33}S$ (2 SD, $n = 43$). All data was blank corrected for the process blanks, and uncertainties were propagated with Monte Carlo simulations. The isotopic composition of the volcanic sulfate was calculated using isotope mass balance and the concentration and isotopic composition of the background ice prior to the volcanic peak in sulfate (57, 59). Uncertainties were propagated with Monte Carlo simulations, and similar to previous studies (59), we found that samples with more than 35% of their sulfate coming from background sources had prohibitively large uncertainties on the volcanic $\delta^{34}S$ and $\Delta^{33}S$ estimates, so were not plotted.

Acknowledgments

We thank the NGRIP, GRIP, and GISP2 communities; M. Twickler, and the NSF-ICF for providing access to archived GISP2 samples; J.P. Steffensen, A. Svensson, and staff from the Niels Bohr Institute, for providing access to archived GRIP and NGRIP samples. Gwydion Jones, Gareth James, Laura Robinson, and Victoria Smith for assistance with the ice-core sampling, tephra preparation, and geochemical work. This work benefited from participation by some authors in the Past Global Changes Volcanic Impacts on Climate and Society working group. M.Si. also thanks Peter Abbott and Eric Wolff. C.P. thanks Peter Brewer, Matthew Salzer, Peter Kuniholm, and David Frank.

Supplementary Material

Supplementary material is available at *PNAS Nexus* online.

Funding

This work was supported by funding from the European Research Council (ERC) under the European Union's Horizon 2020 research and innovation programme (grant agreement 820047 to M.Si.), the Malcolm H. Wiener Foundation (Interdisciplinary Chronology of Civilizations Project to C.P.), and a UKRI Future Leader Fellowship (MR/S035478/1 to P.A).

Author Contributions

C.P., M.Si., and A.B. conceived the experiment(s), analyzed the results, led the writing; A.B. conducted the sulfur isotope analyses; S.D. and A.K. conducted the tephra analyses; M.Se. and J.C. conducted the sulfate analyses; H.I. also conducted the sulfur isotope analyses; P.A. and M.H. also conducted the tephra analysis. All authors contributed to writing of the manuscript.

Data Availability

The data underlying this article are available in full in the Supplementary Material.

References

1. Sigl M, *et al.* 2015. Timing and climate forcing of volcanic eruptions for the past 2,500 years. Nature. 523(7562):543.
2. McConnell JR, *et al.* 2020. Extreme climate after massive eruption of Alaska's Okmok volcano in 43 BCE and effects on the late Roman Republic and Ptolemaic Kingdom. Proc Nat Acad Sci. 117(27):15443–15449.
3. LaMarche VC, Jr, Hirschboeck KK. 1984. Frost rings in trees as records of major volcanic eruptions. Nature. 307(5947):121.
4. Baillie M, Munro MA. 1988. Irish tree rings, Santorini and volcanic dust veils. Nature. 332(6162):344–346.
5. Salzer MW, Hughes MK. 2007. Bristlecone pine tree rings and volcanic eruptions over the last 5000 yr. Quat Res. 67(1):57–68.

6. Salzer MW, Hughes MK. 2010. Volcanic eruptions over the last 5,000 years from high elevation tree-ring widths and frost rings. In: Tree rings and natural hazards, Berlin, Heidelberg: Springer. p. 469–482.
7. McAneney J, Baillie M. 2019. Absolute tree-ring dates for the Late Bronze Age eruptions of Aniakchak and Thera in light of a proposed revision of ice-core chronologies. Antiquity. 93(367): 99–112.
8. Johnston E, Sparks R, Phillips J, Carey S. 2014. Revised estimates for the volume of the Late Bronze Age Minoan eruption, Santorini, Greece. J Geol Soc. 171(4):583–590.
9. Evans K, McCoy F. 2020. Precursory eruptive activity and implied cultural responses to the Late Bronze Age (LBA) eruption of Thera (Santorini, Greece). J Volcanol Geoth Res. 397:106868.
10. Şahoğlu V, *et al.* 2022. Volcanic ash, victims, and tsunami debris from the Late Bronze Age Thera eruption discovered at Çeşme-Bağlararası (Turkey). Proc Nat Acad Sci. 119(1):e2114213118.
11. Warren P. 2010. The date of the Late Bronze Age eruption of Santorini on the basis of the historical chronology. In: DA Warburton, editor. Time's up! Dating the Minoan eruption of Santorini. Athens: Danish Institute at Athens. p. 181–186.
12. Wiener MH. 2010. A point in time. Br Sch Athens Stud. 18: 367–394.
13. Höflmayer F. 2012. The date of the Minoan Santorini eruption: Quantifying the "offset". Radiocarbon. 54(3-4):435–448.
14. Bietak M. 2003. The synchronisation of civilisations in the Eastern Mediterranean in the second millennium BC II. Vienna: Austrian Academy of Sciences Press. Verlag der Österreichischen Akademie der Wissenschaften.
15. Ramsey CB, *et al.* 2010. Radiocarbon-based chronology for dynastic Egypt. Science. 328(5985):1554–1557.
16. Friedrich WL, *et al.* 2006. Santorini eruption radiocarbon dated to 1627–1600 BC. Science. 312(5773):548–548.
17. Manning SW, *et al.* 2014. Dating the Thera (Santorini) eruption: archaeological and scientific evidence supporting a high chronology. Antiquity. 88(342):1164.
18. Van der Plicht J, Ramsey CB, Heaton T, Scott E, Talamo S. 2020. Recent developments in calibration for archaeological and environmental samples. Radiocarbon. 62(4):1095–1117.
19. Pearson CL, *et al.* 2018. Annual radiocarbon record indicates 16th century BCE date for the Thera eruption. Sci Adv. 4(8):eaar8241.
20. Ehrlich Y, Regev L, Boaretto E. 2018. Radiocarbon analysis of modern olive wood raises doubts concerning a crucial piece of evidence in dating the Santorini eruption. Sci Rep. 8(1):1–8.
21. Ehrlich Y, Regev L, Boaretto E. 2021. Discovery of annual growth in a modern olive branch based on carbon isotopes and implications for the Bronze Age volcanic eruption of Santorini. Sci Rep. 11(1):1–11.
22. Zielinski GA, *et al.* 1994. Record of volcanism since 7000 BC from the GISP2 Greenland ice core and implications for the volcano-climate system. Science. 264(5161):948–952.
23. Clausen HB, *et al.* 1997. A comparison of the volcanic records over the past 4000 years from the Greenland Ice Core Project and Dye 3 Greenland ice cores. J Geophys Res Oceans. 102(C12):26707–26723.
24. Vogel JS, Cornell W, Nelson DE, Southon JR. 1990. Vesuvius/Avellino, one possible source of seventeenth century BC climatic disturbances. Nature. 344(6266):534–537.
25. Pearce NJ, Westgate JA, Preece SJ, Eastwood WJ, Perkins WT. 2004. Identification of Aniakchak (Alaska) tephra in Greenland ice core challenges the 1645 BC date for Minoan eruption of Santorini. Geochem Geophys Geosyst. 5(3). DOI: 10.1029/2003GC000672.
26. Abbott PM, Davies SM. 2012. Volcanism and the Greenland ice-cores: the tephra record. Earth Sci Rev. 115(3): 173–191.
27. Coulter SE, *et al.* 2012. Holocene tephras highlight complexity of volcanic signals in Greenland ice cores. J Geophys Res Atmos. 117(D21):D21303.
28. Blackford J, Payne R, Heggen M, de la Riva CA, van der Plicht J. 2014. Age and impacts of the caldera-forming Aniakchak II eruption in western Alaska. Quat Res. 82(1):85–95.
29. Miller TP, Smith RL. 1987. Late quaternary caldera-forming eruptions in the eastern Aleutian arc, Alaska. Geology. 15(5): 434–438.
30. Pearce C, *et al.* 2017. The 3.6 ka Aniakchak tephra in the Arctic Ocean: a constraint on the Holocene radiocarbon reservoir age in the Chukchi Sea. Clim Past. 13(4):303–316.
31. Mayewski PA, *et al.* 1997. Major features and forcing of high-latitude Northern Hemisphere atmospheric circulation using a 110,000-year-long glaciochemical series. J Geophys Res Oceans. 102(C12):26345–26366.
32. Wolff EW, Moore JC, Clausen HB, Hammer CU. 1997. Climatic implications of background acidity and other chemistry derived from electrical studies of the Greenland Ice Core Project ice core. J Geophys Res Oceans. 102(C12):26325–26332.
33. Mojtabavi S, *et al.* 2020. A first chronology for the East Greenland Ice-core Project (EGRIP) over the Holocene and last glacial termination. Clim Past. 16(6):2359–2380.
34. Sigl M, *et al.* 2016. The WAIS divide deep ice core WD2014 chronology–Part 2: annual-layer counting (0–31 ka BP). Clim Past. 12(3):769–786.
35. Cole-Dai J, *et al.* 2021. Comprehensive record of volcanic eruptions in the Holocene (11,000 years) from the WAIS Divide, Antarctica ice core. J Geophys Res Atmos. 126(7):e2020JD032855.
36. Severi M, *et al.* 2007. Synchronisation of the EDML and EDC ice cores for the last 52 kyr by volcanic signature matching. Clim Past. 3(3):367–374.
37. Hammer CU, Clausen HB, Friedrich WL, Tauber H. 1987. The Minoan eruption of Santorini in Greece dated to 1645 BC?. Nature. 328(6130):517–519.
38. Zielinski GA, Mayewski PA, Meeker LD, Whitlow S, Twickler MS. 1996. A 110,000-yr record of explosive volcanism from the GISP2 (Greenland) ice core. Quat Res. 45(2):109–118.
39. Plunkett G, *et al.* 2017. Trace element analysis of Late Holocene tephras from Greenland ice cores. Quat Newsl. 143: 10–20.
40. Hantemirov RM, Shiyatov SG. 2002. A continuous multimillennial ring-width chronology in Yamal, northwestern Siberia. Holocene. 12(6):717–726.
41. Wiener MH. 2015. Dating the Theran Eruption: archaeological science versus nonsense science. In: Israel's exodus in transdisciplinary perspective. Berlin, Heidelberg: Springer. p. 131–143.
42. Helama S, *et al.* 2019. Frost rings in 1627 BC and AD 536 in subfossil pinewood from Finnish Lapland. Quat Sci Rev. 204:208–215.
43. Pearson C, *et al.* 2020. Securing timelines in the ancient Mediterranean using multiproxy annual tree-ring data. Proc Nat Acad Sci. 117(15):8410–8415.
44. Grudd H, Briffa KR, Gunnarson BE, Linderholm HW. 2000. Swedish tree rings provide new evidence in support of a major, widespread environmental disruption in 1628 BC. Geophys Res Lett. 27(18):2957–2960.
45. Sigl M, *et al.* 2013. A new bipolar ice core record of volcanism from WAIS Divide and NEEM and implications for climate forcing of the last 2000 years. J Geophys Res-Atmos. 118(3):1151–1169.

46. Burke A, *et al.* 2019. Stratospheric eruptions from tropical and extra-tropical volcanoes constrained using high-resolution sulfur isotopes in ice cores. Earth Planet Sci Lett. 521: 113–119.
47. Vinther BM, *et al.* 2006. A synchronized dating of three Greenland ice cores throughout the Holocene. J Geophys Res Atmos. 111(D13). DOI: 10.1029/2005JD006921.
48. Meese D, *et al.* 1997. The Greenland Ice Sheet Project 2 depth-age scale: methods and results. J Geophys Res Oceans. 102(C12):26411–26423.
49. Adolphi F, Muscheler R. 2016. Synchronizing the Greenland ice core and radiocarbon timescales over the Holocene–Bayesian wiggle-matching of cosmogenic radionuclide records. Clim Past. 12(1):15–30.
50. Sigl M, *et al.* 2014. Insights from Antarctica on volcanic forcing during the Common Era. Nat Clim Change. 4(8):693–697.
51. Toohey M, Sigl M. 2017. Volcanic stratospheric sulfur injections and aerosol optical depth from 500 BCE to 1900 CE. Earth Syst Sci Data. 9(2):809–831.
52. Gao C, Oman L, Robock A, Stenchikov GL. 2007. Atmospheric volcanic loading derived from bipolar ice cores: accounting for the spatial distribution of volcanic deposition. J Geophys Res-Atmos. 112(D9). DOI: 10.1029/2006JD007461.
53. Abbott P, *et al.* 2021. Community established best practice recommendations for tephra studies-from collection through analysis (version 3.0. 0). Zenodo. data set.
54. Iverson NA, Kalteyer D, Dunbar NW, Kurbatov A, Yates M. 2017. Advancements and best practices for analysis and correlation of tephra and cryptotephra in ice. Quat Geochronol. 40:45–55.
55. Abbott PM, *et al.* 2012. A detailed framework of Marine Isotope Stages 4 and 5 volcanic events recorded in two Greenland ice-cores. Quat Sci Rev. 36:59–77.
56. Savarino J, Romero A, Cole-Dai J, Bekki S, Thiemens M. 2003. UV induced mass-independent sulfur isotope fractionation in stratospheric volcanic sulfate. Geophys Res Lett. 30(21):2131.
57. Baroni M, Thiemens MH, Delmas RJ, Savarino J. 2007. Mass-independent sulfur isotopic compositions in stratospheric volcanic eruptions. Science. 315(5808):84–87.
58. Burke A, *et al.* 2018. Sulfur isotopes in rivers: insights into global weathering budgets, pyrite oxidation, and the modern sulfur cycle. Earth Planet Sci Lett. 496:168–177.
59. Gautier E, Savarino J, Erbland J, Farquhar J. 2018. SO_2 oxidation kinetics leave a consistent isotopic imprint on volcanic ice core sulfate. J Geophys Res Atmos. 123(17):9801–9812.
60. Seierstad IK, *et al.* 2014. Consistently dated records from the Greenland GRIP, GISP2 and NGRIP ice cores for the past 104 ka reveal regional millennial-scale δ18O gradients with possible Heinrich event imprint. Quat Sci Rev. 106:29–46.
61. Oppenheimer C. 2003. Climatic, environmental and human consequences of the largest known historic eruption: Tambora volcano (Indonesia) 1815. Prog Phys Geog. 27(2):230–259.
62. Wallace KL, Hayden LA, Neal C. 2017. Major-element glass compositions of Tephra from the Circa 3.6 Ka eruption of Aniakchak Volcano, Alaska Peninsula, Alaska.. Fairbanks (AK): State of Alaska, Alaska Division of Geological and Geophysical Surveys. State of Alaska, Department of Natural Resources, Division of Geological.
63. Wulf S, *et al.* 2020. Advancing Santorini's tephrostratigraphy: new glass geochemical data and improved marine-terrestrial tephra correlations for the past 360 kyrs. Earth Sci Rev. 200:102964.
64. Jochum KP, *et al.* 2006. MPI-DING reference glasses for in situ microanalysis: New reference values for element concentrations and isotope ratios. Geochem Geophys Geosyst. 7(2). DOI: 10.1029/2005GC001060.
65. Jarosewich E, Nelen J, Norberg JA. 1980. Reference samples for electron microprobe analysis. Geostandard Newslett. 4(1):43–47.
66. Dunbar NW, *et al.* 2017. New Zealand supereruption provides time marker for the Last Glacial Maximum in Antarctica. Sci Rep. 7(1):1–8.
67. Herren PA, *et al.* 2013. The onset of Neoglaciation 6000 years ago in western Mongolia revealed by an ice core from the Tsambagarav mountain range. Quat Sci Rev. 69:59–68.
68. Marshall L, *et al.* 2018. Multi-model comparison of the volcanic sulfate deposition from the 1815 eruption of Mt. Tambora. Atmos Chem Phys. 18(3):2307–2328.
69. Jensen BJ, Beaudoin AB, Clynne MA, Harvey J, Vallance JW. 2019. A re-examination of the three most prominent Holocene tephra deposits in western Canada: Bridge River, Mount St. Helens Yn and Mazama. Quat Int. 500:83–95.
70. Carey S, Gardner J, Sigurdsson H. 1995. The intensity and magnitude of Holocene Plinian eruptions from Mount St. Helens volcano. J Volcanol Geoth Res. 66(1-4):185–202.
71. Zielinski GA. 1998. Reply to: correction. New GISP2 ice-core evidence supports 17th century BC date for the Santorini (Minoan) eruption. J Archaeol Sci. 25(10):1043–1045.
72. Cadoux A, Scaillet B, Bekki S, Oppenheimer C, Druitt TH. 2015. Stratospheric ozone destruction by the Bronze-Age Minoan eruption (Santorini volcano, Greece). Sci Rep. 5(1):1–12.
73. Panagiotakopulu E, Higham T, Sarpaki A, Buckland P, Doumas C. 2013. Ancient pests: the season of the Santorini Minoan volcanic eruption and a date from insect chitin. Naturwissenschaften. 100(7):683–689.
74. Marshall L, *et al.* 2019. Exploring how eruption source parameters affect volcanic radiative forcing using statistical emulation. J Geophys Res Atmos. 124(2):964–985.
75. Badertscher S, *et al.* 2014. Speleothems as sensitive recorders of volcanic eruptions–the Bronze Age Minoan eruption recorded in a stalagmite from Turkey. Earth Planet Sci Lett. 392:58–66.
76. Warren P. 1984. Archaeology: absolute dating of the Bronze Age eruption of Thera (Santorini). Nature. 308(5959):492–493.
77. Salzer MW, Larson ER, Bunn AG, Hughes MK. 2014. Changing climate response in near-treeline bristlecone pine with elevation and aspect. Environ Res Lett. 9(11):114007.
78. Palais JM, Sigurdsson H. 1989. Petrologic evidence of volatile emissions from major historic and pre-historic volcanic eruptions. Underst Clim Change Geophys Monogr Ser. 52: 31–53.
79. Ponomareva V, *et al.* 2018. Holocene tephra from the Chukchi-Alaskan margin, Arctic Ocean: implications for sediment chronostratigraphy and volcanic history. Quat Geochronol. 45:85–97.
80. Begét J, Mason O, Anderson P. 1992. Age, extent and climatic significance of the c. 3400 BP Aniakchak tephra, western Alaska, USA. Holocene. 2(1):51–56.
81. Denton JS, Pearce NJ. 2008. Comment on "A synchronized dating of three Greenland ice cores throughout the Holocene" by BM Vinther et al.: no Minoan tephra in the 1642 BC layer of the GRIP ice core. J Geophys Res. 113(D4):D04303.
82. Toohey M, *et al.* 2019. Disproportionately strong climate forcing from extratropical explosive volcanic eruptions. Nat Geosci. 12(2):100–107.
83. Kobashi T, *et al.* 2017. Volcanic influence on centennial to millennial Holocene Greenland temperature change. Sci Rep. 7(1):1–10.
84. Pyle DM. 1990. New estimates for the volume of the Minoan eruption. Thera Aegean World III. 2:113–121.

85. Eastwood WJ, Pearce NJ, Westgate JA, Perkins WT. 1998. Recognition of Santorini (Minoan) tephra in lake sediments from Gölhisar Gölü, southwest Turkey by laser ablation ICP-MS. J Archaeol Sci. 25(7):677–687.
86. Bottema S, Sarpaki A. 2003. Environmental change in Crete: a 9000-year record of Holocene vegetation history and the effect of the Santorini eruption. Holocene. 13(5):733–749.
87. Kern Z, Demény A, Perşoiu A, Hatvani IG. 2019. Speleothem records from the eastern part of Europe and Turkey—discussion on stable oxygen and carbon isotopes. Quaternary. 2(3):31.
88. Jørgensen EK, Riede F. 2019. Convergent catastrophes and the termination of the Arctic Norwegian Stone Age: a multiproxy assessment of the demographic and adaptive responses of mid-Holocene collectors to biophysical forcing. Holocene. 29(11):1782–1800.
89. de Jong T, Foertmeyer V. 2010. A new look at the Venus observations of Ammisaduqa: traces of the Santorini eruption in the atmosphere of Babylon. Jaarbericht van het Vooraziatisch-Egyptisch Genootschap Ex Oriente Lux. 42: 143–59.